AGU PUBLICATIONS

JGR

Journal of Geophysical Research: Atmospheres

RESEARCH ARTICLE
10.1002/2015JD023648

Key Points:
- BC aerosols were measured over the Bering Sea, Arctic, and North Pacific Oceans
- BC mass concentrations (September 2014) over the Arctic Ocean were 1.0 ± 1.2 ng/m^3
- Nonshell/noncore structure particles contributed to mixed BC over the Arctic Ocean

Supporting Information:
- Figures S1 and S2

Correspondence to:
F. Taketani,
taketani@jamstec.go.jp

Citation:
Taketani, F., T. Miyakawa, H. Takashima, Y. Komazaki, X. Pan, Y. Kanaya, and J. Inoue (2016), Shipborne observations of atmospheric black carbon aerosol particles over the Arctic Ocean, Bering Sea, and North Pacific Ocean during September 2014, *J. Geophys. Res. Atmos.*, *121*, 1914–1921, doi:10.1002/2015JD023648.

Received 14 JUL 2015
Accepted 24 DEC 2015
Accepted article online 4 JAN 2016
Published online 19 FEB 2016

Shipborne observations of atmospheric black carbon aerosol particles over the Arctic Ocean, Bering Sea, and North Pacific Ocean during September 2014

Fumikazu Taketani[1,2], Takuma Miyakawa[1,2], Hisahiro Takashima[1,3], Yuichi Komazaki[1], Xiaole Pan[4], Yugo Kanaya[1,2], and Jun Inoue[2,5]

[1]Department of Environmental Geochemical Cycle Research, Japan Agency for Marine-Earth Science and Technology, Yokohama, Japan, [2]Institute of Arctic Climate and Environment Research, Japan Agency for Marine-Earth Science and Technology, Yokosuka, Japan, [3]Department of Earth System Science, Faculty of Science, Fukuoka University, Fukuoka, Japan, [4]Center for Integrated Atmospheric Environment Research, Kyushu University, Fukuoka, Japan, [5]National Institute of Polar Research, Tokyo, Japan

Abstract Measurements of refractory black carbon (rBC) aerosol particles using a highly sensitive online single particle soot photometer were performed on board the R/V *Mirai* during a cruise across the Arctic Ocean, Bering Sea, and North Pacific Ocean (31 August to 9 October 2014). The measured rBC mass concentrations over the Arctic Ocean in the latitudinal region > 70°N were in the range 0–66 ng/m^3 for 1 min averages, with an overall mean value of 1.0 ± 1.2 ng/m^3. Single-particle-based observations enabled the measurement of such low rBC mass concentrations. The effects of long-range transport from continents to the Arctic Ocean were limited during the observed period, which suggests that the low rBC concentration levels would prevail over the Arctic Ocean. An analysis of rBC mixing states showed that particles with a nonshell/noncore structure made a significant contribution to the rBC particles detected over the Arctic Ocean.

1. Introduction

Black carbon (BC), which is formed through the incomplete combustion of fossil fuels, biofuels, and biomass, has positive radiative forcing properties and is a major component of light-absorbing particulate matter in the atmosphere [*Bond et al.*, 2013; *Jacobson*, 2001]. In northern high-latitude regions (e.g., > 65°N), BC can reduce the snow/sea ice surface albedo upon deposition by absorbing sunlight, thereby accelerating melting and affecting the Arctic climate system [*Quinn et al.*, 2008, 2011]. Through these processes, BC changes the regional radiative balance; therefore, several research groups have conducted measurements of BC in the ambient atmosphere of Arctic regions, together with model calculations, to investigate the influence of BC on climate [*Eleftheriadis et al.*, 2009; *Flanner et al.*, 2009; *Flanner*, 2013; *McConnell et al.*, 2007; *Schwarz et al.*, 2010, 2013; *Sharma et al.*, 2006, 2013; *Stone et al.*, 2014]. In particular, climate simulations have indicated that BC residing in the lowest level of the atmosphere induces strong Arctic warming per unit mass and forcing [*Flanner*, 2013]. Measurements of BC in central Greenland ice cores have been used to determine the source of BC in snow over the past 200 years. The results indicated that the BC deposited in Greenland snow primarily originated from industrial activity in North America and Asia, and from forest fires [*Keegan et al.*, 2014; *McConnell et al.*, 2007].

Long-term ground-based observations of BC in the Arctic region have been performed at Barrow, Alaska (71°N, 156.6°W); Alert, Canada (82.39°N, 62.3°W); and Zeppelin, Norway (78.88°N, 11.88°E) [*Eleftheriadis et al.*, 2009; *Sharma et al.*, 2006, 2013]. Clear seasonal variations in BC were reported, with maxima in winter and minima in summer. These data from ground-based measurements have been compared with regional and global model simulations [e.g., *Liu et al.*, 2011]. There would be several factors such as transportation, removal process, and vertical mixing, to contribute the BC concentrations in winter. For example, trajectory analyses for winter conditions [e.g., *Sharma et al.*, 2013] showed that the BC at Barrow from anthropogenic combustion processes at midlatitudes (e.g., Asia and Russia) should be transported to the Arctic. The lower BC concentrations during summer than in winter might be caused by reduced transportation from BC source regions due to the migration of the Arctic front [*Sharma et al.*, 2013]. These studies indicated that BC concentrations in the Arctic region are highly dependent on air mass origin.

To our knowledge, there has only been one previous summertime study of ship-based BC measurements over the Arctic Ocean [*Sierau et al.*, 2014]. In that study, the BC number concentration was only indirectly

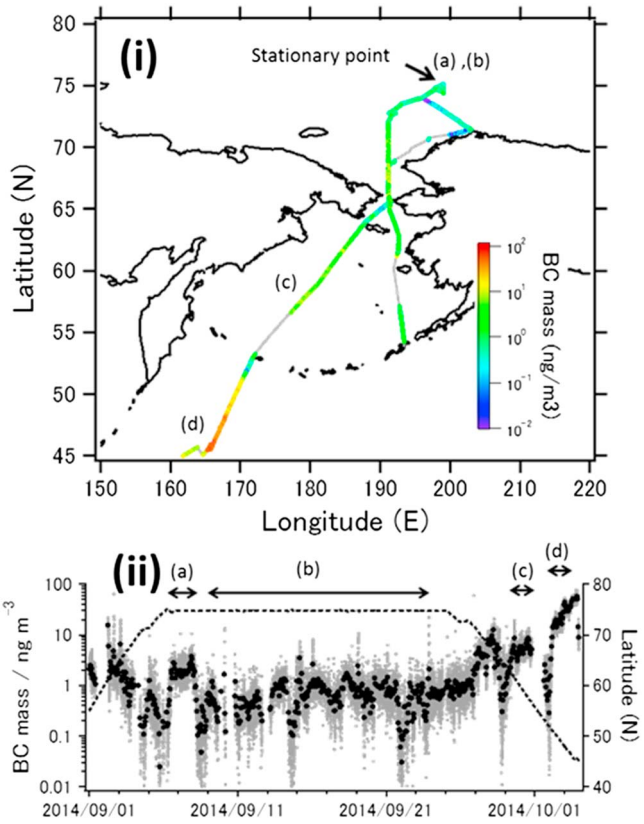

Figure 1. (top) Distribution and (bottom) time-dependent variations of refractory black carbon (rBC) mass concentrations over the surface of the Arctic Ocean, Bering Sea, and North Pacific Ocean along the cruise track. In Figure 1 (top), the gray line shows the cruise track, and the colors on this track line indicate the rBC mass concentrations. In Figure 1 (bottom), the gray and black dots show the BC mass concentration averaged at 1 min and 1 h, respectively. Points with horizontal arrow bars, marked (a)–(d), indicate the four BC periods focused on in this study.

determined using a passive cavity aerosol spectrometer probe (PCASP) combined with a heating system (particles lost by heating from 620 to 650°C were regarded as BC particles). Recently, *Raatikainen et al.* [2015] reported ground-based observations of BC mass size distribution and mixing state in the Finnish Arctic during wintertime using a single particle soot photometer (SP2). The authors indicated that most BC particles had undergone long-range transport from the south and that they had an average geometric mass mean diameter of 194 nm and a typical shell/core ratio of ~2. Aircraft-borne measurements of BC have also been conducted to obtain information on vertical profiles over the Arctic [*Kondo et al.*, 2011; *Matsui et al.*, 2011; *Schwarz et al.*, 2010, 2013; *Spackman et al.*, 2010]. These studies indicated that the altitude dependence of BC concentrations is strongly affected by season and by the origin of the air mass. Furthermore, on average, the model, i.e., the AeroCom ensemble mean [*Myhre et al.*, 2013], overestimated the observed mass concentrations of BC by a factor of 4 [*Schwarz et al.*, 2013], suggesting a large uncertainty within the removal processes of BC in this model.

To understand the effect of BC on the Arctic climate, the determination of BC mass concentrations and their mixing states over the Arctic Ocean is essential and will provide information on loss processes and radiative forcing properties. On this basis, we performed direct measurements of refractory BC (rBC) over the Arctic Ocean using an SP2 instrument during a cruise of the R/V *Mirai* across the Arctic region.

2. Measurement and Analysis Methods

Observations were conducted on board the R/V *Mirai* from 31 August 2014 to 9 October 2014, between the ports of Dutch Harbor, Alaska, USA (53.90°N, 166.53°W), and Yokohama Port (35.45°N, 139.64°W), Kanagawa, Japan, via the Arctic Ocean. Figure 1 (top) shows the trace of the research cruise. Moreover, observations were carried out at a stationary point in the Arctic Ocean (74.75°N, 162.00°W) from 6 to 25 September 2014.

Measurements of atmospheric rBC particles were conducted using the SP2 instrument (Droplet Measurement Technologies, Inc., CO, USA). We employed the notation of "refractory BC" (rBC), as recommended by previous studies [*Petzold et al.*, 2013; *Schwarz et al.*, 2010]. SP2 is based on the laser-induced incandescence (LII) method [*Moteki and Kondo*, 2007; *Schwarz et al.*, 2006]. Ambient particles were sampled using a PM-10 inlet (URG-2000-DBQ) installed on the flying bridge, ~18 m above sea level, through a 3 m long conductive tube and a diffusion dryer (3062, TSI, Inc., MN, USA). After passing through the dryer, the flow was separated into two lines. One line was for a bypass vent flow, whose volumetric flow rate was 2.5 L/min, while the other was further separated into two lines for SP2 (0.1 L/min) and for monitoring the relative humidity (RH) of

the flow 0.2 L/min. During the cruise, the RH remained below 30% at room temperature. Leakage from the SP2 chamber was tested by outfitting an High-efficiency particulate arrestance filter and was found to be negligible. The ambient particle losses inside the diffusion dryer with the sampling tube were quantified to be ~10% for the size range 100–500 nm and were corrected.

Calibration of the SP2 was performed before the cruise. We investigated the relationship between electrical mobility diameter (D_{mob}) and laser-induced incandescence (LII) signal intensities (S_{LII}) using laboratory-generated fullerene soot particles (FS; stock 40971, lot L20W054, Alfa Aesar, USA). The FS particles, which were classified by size using a differential mobility analyzer (DMA model 3080, TSI Inc., USA), were introduced into the SP2. We separately investigated the relationship between rBC mass per FS particle (m_{PP}) and its D_{mob} using an aerosol particle mass analyzer (APM model 3601; Kanomax Japan, Inc., Japan) [*Ehara et al*., 1996], coupled in tandem to a DMA [*Moteki and Kondo*, 2010]. Combining the two relationships, D_{mob}-S_{LII} and m_{PP}-D_{mob}, enables us to quantify the FS-equivalent rBC mass per particle from the observed S_{LII} for an rBC-containing particle in the atmosphere. This calibration method yielded a reasonable agreement ($<$ ~30%) in the mass concentration between rBC and elemental carbon measured using a semicontinuous carbon analyzer (Sunset Laboratory, Inc., USA) in an industrial area of Japan, as discussed by T. Miyakawa (manuscript in review, 2015). The size of the rBC particle was derived by assuming sphericity and a fixed density of 1.8 g/cm^3. Hereafter, we use the mass equivalent diameter (MED, D_{BC}) when referring to the size of the rBC particles.

To avoid the influence of ship exhaust (the ship's funnel is located at the rear of sampling inlet), we only used data (61% of the total) recorded when the wind direction and speed (as determined by the R/V system) relative to the ship's course were within ±60° from the bow and $>$ 3 m/s, respectively.

The mixing state of rBC-containing particles was qualitatively estimated by using the lag time of the LII peak with respect to the peak of the scattering signal. Moreover, the coating thicknesses of the rBC-containing particles were calculated using the leading edge only (LEO) fitting method [*Gao et al*., 2007]. Normally, the LEO fitting method is performed using "leading edge" data before a particle is exposed to 1–5% of the maximum laser intensity. A strict threshold (e.g., 1%) may reduce the risk of the onset of evaporation of the coating. However, it can also lead to the possibility of incorrect estimation of the scattering peak height by Gaussian fitting. In this study, the leading edge data were selected using the normalized time derivative method, as proposed by *Moteki and Kondo* [2007], to extract the data before the coating material on the rBC-containing particle evaporated. The temporal behavior of the ratio of the time derivative logarithm of the scattering amplitude to the normalized time derivative of the laser intensity profile, which was obtained using the polystyrene latex particles, was employed. The particle location relative to the laser center was adjusted by using splitting point data. The temporal profile of the ratio is linear only in the absence of any material loss. When the temporal profile of the ratio deviated from its original course, the onset of evaporation was indicated by a sudden decrease in the scattering amplitude after evaporation. In this manner, the data for the leading edge were selected. Full details are described in X.-L. Pan (manuscript in preparation, 2015).

To analyze the morphology and components of individual particles via a transmission electron microscope (TEM) utilizing energy-dispersive X-ray (EDX) spectroscopy, we performed sampling of the ambient aerosol particles using a three-stage particle sampler (MPS-3; California Measurement, Inc., CA, USA) with a flow rate of 3 L/min set on the flying deck. Aerosol particles were collected onto copper grids with a microgrid support film. The sampling time periods were 60–90 min. To acquire representative individual aerosol particle images, we used a Tecnai 20 TEM (FEI Co., OR, USA) with a 200 kV acceleration voltage.

The CO mixing ratio was also measured using a nondispersive infrared CO gas analyzer (Thermo Scientific, Model 48C, USA, flow rate: 1 L/min) equipped with a Teflon. Ambient air was sampled at the flying bridge and introduced to the instrument via the Teflon tube. The zero level (the baseline of the instrumental signal) was routinely determined in the first 20 min of each hour using purified air supplied by a zero gas generator (Model 96, Nippon Thermo Co., Ltd., Japan) operated at ambient humidity. The instrument was calibrated using a standard gas cylinder (CO/N_2: 1.05 ppm) before and after the cruise.

To investigate potential source regions and transport pathways of the rBC particles, 5 day backward trajectories were calculated every hour, with the starting points 500 m above the cruise track, using a kinematic model employing the European Centre for Medium-Range Weather Forecasts-Interim data set, with a spatial resolution of 1.5° × 1.5° (longitude × latitude grid) [*Dee et al*., 2011; *Takashima et al*., 2008].

3. Results and Discussion

3.1. Mass Concentration of rBC

Figure 1 shows (top) the geographical distribution and (bottom) the time series of the rBC mass concentrations observed over the Arctic Ocean, Bering Sea, and North Pacific Ocean during the cruise. The range in rBC concentrations spanned 4 orders of magnitude (10^{-2}–10^{2} ng/m^3); those measured in the Arctic region were the lowest. The mean rBC concentration over the Arctic Ocean in the latitudinal region $>$ 70°N was 1.0 ± 1.2 ng/m^3, based on the 1 min averages. From 6 to 25 September, observations were carried out at a stationary point. Relatively high rBC concentrations were observed on 7–8 September, while the rBC concentrations were lower during 9–25 September. In this study, we focused on four cases ((a)–(d); Figure 1) of rBC observations, which were made over the Arctic Ocean ((a) = 7–8 September; (b) = 9–24 September), the Bering Sea ((c) = 29 September), and the North Pacific Ocean ((d) = 3 October). To identify the air mass origins for each case, 5 day back trajectories of the rBC concentration levels were performed (Figure S1 in the supporting information). The results indicated that on 7–8 September, the air mass originated from south/west (the continent) and traveled in short periods from the continent to the observed location, whereas the air mass on 9–24 September was from the east and/or north (the ocean). These results indicate that even at such low concentration levels, rBC concentrations are very sensitive to the air mass traveling route and time to the observed location from the continent. Based on the trajectory analysis, it can be concluded that the influence of long-range transport from the continent was limited during 9–25 September (Figure S1), which suggests that such low rBC concentration levels (0.79 ± 0.80 ng/m3) would prevail over the Arctic Ocean.

The CO mixing ratio at $>$ 70°N, calculated for 1 h averages, was almost stable (112 ± 7 ppbv; Figure S2). The relationship between rBC and the excess CO subtracted background CO value (ΔCO) is useful for determining source information. However, in this study, it was difficult to determine ΔrBC/ΔCO due to the poor correlation between the rBC mass and CO mixing ratio due to the contribution of rBC removal.

There are very few comparable data sets that have been obtained in the Arctic region during the summertime. Using PCASP, *Sierau et al*. [2014] estimated the BC number concentration (as particles lost by heating from 620 to 650°C) to be in a very low range (0–5 particles cm^{-3}), which closely agrees with our direct measurements, where the rBC number concentrations were 0–2 particles cm^{-3} for the 1 h averages during 7–25 September. Moreover, aircraft observations of the rBC particles at 72°N and 146°W, which were made during HIPPO5 using an SP2 instrument [*Schwarz et al*., 2013], yielded ~0.7 ng/m^3 at an altitude of 400–600 m in August 2011 [*Wofsy et al*., 2012], which is also in good agreement with our results (1.0 ng/m^3). Considering that airborne data were obtained over a short period (a few minutes), our rBC results are the first to evaluate such low mass concentration levels from longer term observations over the Arctic Ocean at surface levels. *Sharma et al*. [2006, 2013] performed long-term ground-based observations of the BC concentrations at Barrow (71°N, 156.6°W), at a location ~450 km from the ship's position, on 6–25 September. Their data show strong seasonal trends; in summer, BC concentrations are at their lowest (~10 ng/m^3). However, this concentration level is still much higher than that of our results (1.0 ng/m^3). There are several possibilities that can explain these differences. For example, the discrepancy may be related to the difference in the measuring instruments used and/or location. An aethalometer, which was used at Barrow, is based on optical absorption measurements and can be positively biased, by a factor of 2.5–5 [*Raatikainen et al*., 2015; *Wang et al*., 2014], by non-BC species. The artifact by scattering effect in the aethalometer also may be contributed. At the ground-based site, local emissions, even when weak, may also affect the BC mass observations. Although more measurements are required before reaching a conclusion, our results to date indicate that BC concentrations over the Arctic Ocean were lower than those recorded by the ground-based observation at Barrow. The concentrations of rBC over the Bering Sea (55–60°N) and the North Pacific Ocean (45–53°N) were higher than those in the Arctic, with values of 6.0 ± 1.9 and 24 ± 19 ng/m^3, respectively. These higher values were attributed to influences from the Eurasian continent (Figure S1).

3.2. Size Distribution of rBC

Figure 2 shows the normalized mass size distribution of the rBC measured for the four cases. The rBC mass fraction outside the lower and upper size boundaries that was missed by SP2 detection was small (2–10%), as estimated by fitting a lognormal distribution to the observed rBC size distribution, which indicated that

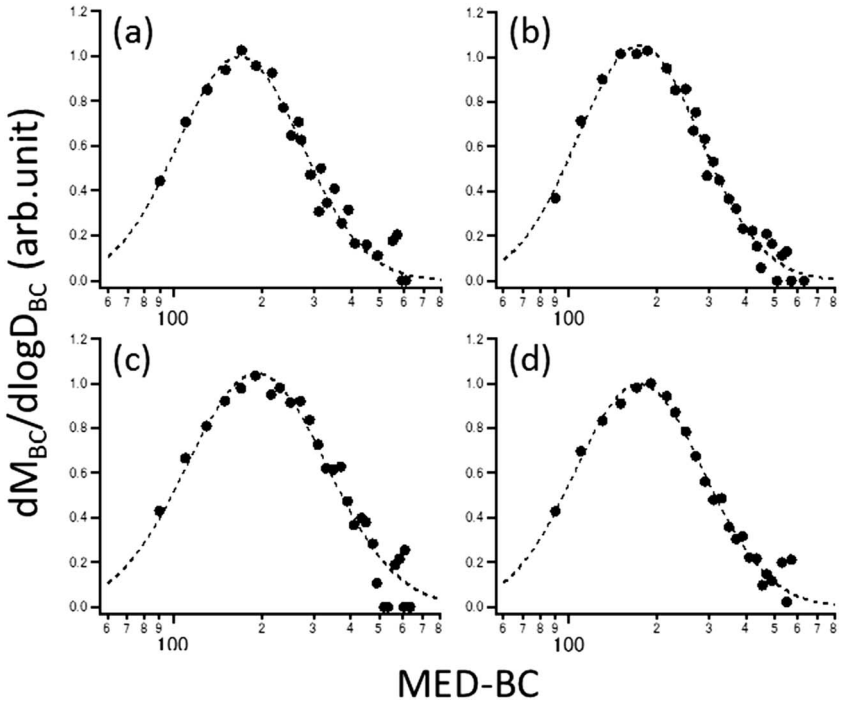

Figure 2. Normalized mass distributions of the refractory black carbon (rBC) component of ambient aerosol particles over the Arctic Ocean, Bering Sea, and North Pacific Ocean. (a–d) The cases for each period marked in Figure 1. The dashed lines denote lognormal fits to the observed results using the data from 90 to 400 nm of MED-BC.

almost all of the rBC was detected by the SP2. The median value of rBC MED (MMD) and the corresponding geometric standard deviations (σ_g) are summarized in Table 1. In the Arctic region (cases (a) and (b)), the median values of MED were ~170 nm. The medians of the rBC MED over the Bering Sea and the North Pacific Ocean were also in the range of 170–190 nm, which suggested that this BC size was dominant in the observed masses of this cruise.

3.3. Mixing State of rBC

The lag time (Δt) distributions for $D_{BC} = 190 \pm 30$ nm for the four cases are depicted in Figure 3. Δt is a useful indicator of the mixing state of the rBC-containing particles. Significant peaks at approximately −3, 0.5, and 2.5 μs were recorded over the Arctic Ocean, whereas only the 0.5 and 2.5 μs peaks were detected over the Bering Sea and the North Pacific Ocean. The contributions (in each case) from the peak areas at approximately −3, 0.5, and 2.5 μs are also listed in Table 1. In our laboratory experiment, the Δt values of the uncoated fullerene soot particles employed in the calibration were 0.8 ± 0.5 μs, which indicated that uncoated BC particles should be in this range. Hence, the peak center (Δt_c) at ~0.5 μs was suggestive of uncoated and/or very thinly coated rBC, whereas the peak at ~2.5 μs was likely thickly coated rBC [*Moteki and Kondo*, 2007]. This finding suggests that for all cases, more than 50% of the rBC particles ($D_{BC} = 190 \pm 30$ nm) were coated. In the Arctic Ocean, the fraction of uncoated and/or very thinly coated rBC with a peak at approximately 0.5 μs was higher for case (a) than for case (b), which is consistent with our previous interpretation that the air mass from the

Table 1. Size Distribution and Lag Time Contribution of Observed rBC

	MMD[a] (nm)	σ_g	Area 1 (Δt_c[b] = −3 μs)	Area 2 (Δt_c = 0.5 μs)	Area 3 (Δt_c = 2.5 μs)
(a)	168 ± 4	1.80	0.18	0.30	0.52
(b)	173 ± 2	1.79	0.19	0.19	0.62
(c)	192 ± 5	1.86	0.02	0.42	0.56
(d)	173 ± 2	1.82	0.01	0.24	0.75

[a]MMD is the median value of refractory black carbon (rBC) MED by lognormal fitting.
[b]Δt_c is the position of the peak center in the lag time distribution.

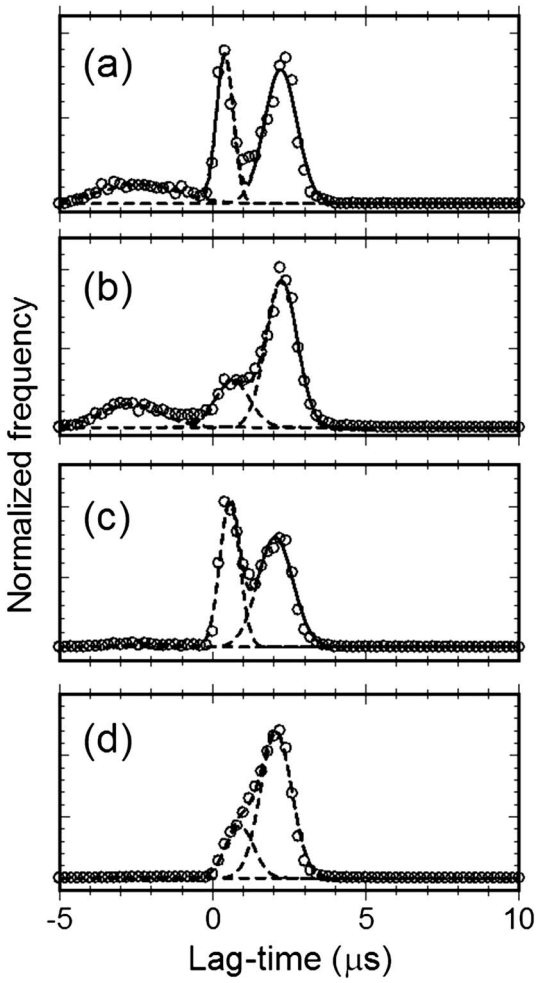

Figure 3. Normalized lag time distributions of refractory black carbon (rBC) for $D_{BC} = 190 \pm 30$ nm and for each period marked in Figure 1. Gaussian fitting (dashed lines) was used to obtain these results. Values indicate the normalized contributions for the three peaks at approximately −3, 0.5, and 2.5 μs, which imply a nonshell/noncore rBC structure, an uncoated and/or very thinly coated structure, and a thickly coated structure, respectively.

south, which was involved in case (a), contained fresh BC. The differences in contributions of uncoated and/or very thinly coated rBC during events (c) and (d) might be attributed to the distance from the continent.

Over the Arctic Ocean, significant negative peaks at approximately −3 μs were detected (cases (a) and (b)), which implied that the rBC particles had a "nonshell/noncore structure," meaning that there was rBC located on/near the surface of the particles. These may have fragmented into rBC and non-BC particles in the laser beam [*Sedlacek et al.*, 2012] due to the localization of rBC. Such rBC particles were not detected over the Bering Sea and the North Pacific Ocean, while they contributed ~20% to the rBC over the Arctic Ocean. The mass absorption cross section of an individual BC-containing particle depends on its morphology, mass, and amount of internally mixed non-BC compounds [*Adachi et al.*, 2010]. Thus, information on mixing status, as provided by our observations, was critical when estimating of the regional radiative balance. Particles of rBC with a nonshell/noncore structure have only been reported in air masses influenced by biomass burning or urban plumes [*Adachi et al.*, 2010; *Dahlkötter et al.*, 2014; *Moteki et al.*, 2014; *Sedlacek et al.*, 2012]. The results from this study represent the first reported case from very clean air.

We also performed analysis of the morphology and components of these particles using TEM-EDX. Figure 4 shows TEM images of bare, shell/core, and nonshell/noncore BC collected over the Arctic Ocean. Even at low BC concentration levels, we found that several BC particles were attached to the surfaces of non-BC material in addition to bare and coated BC via TEM-EDX analysis. These non-BC materials typically consisted of Na, S, O, and Cl. From these constituents and the particle shapes [*Chi et al.*, 2015], we inferred that the attached non-BC material was likely sea salt, suggesting that such particles could have been produced by coagulation. The statistical analysis for the mixing state of BC was difficult to conduct in this study due to the low BC particle concentration and short sampling time and will be addressed in future work. However, our offline microscopic observations qualitatively supported the SP2-based online observations of the nonshell-/noncore-structured rBC.

For particles with lag time $\Delta t > 0$ μs, the ratios of the particle shell diameter (D_p), estimated with the LEO fitting method, to the core size of $D_{BC} = 190 \pm 30$ nm were determined to be 1.6 ± 0.3, 1.5 ± 0.3, and 1.5 ± 0.4 over the Arctic Ocean, Bering Sea, and North Pacific Ocean, respectively. Our results indicate that the BC coating over the Arctic Ocean Bering Sea and North Pacific Ocean was almost same and will have had a larger impact on the lensing effect [*Adachi et al.*, 2010; *Shiraiwa et al.*, 2010].

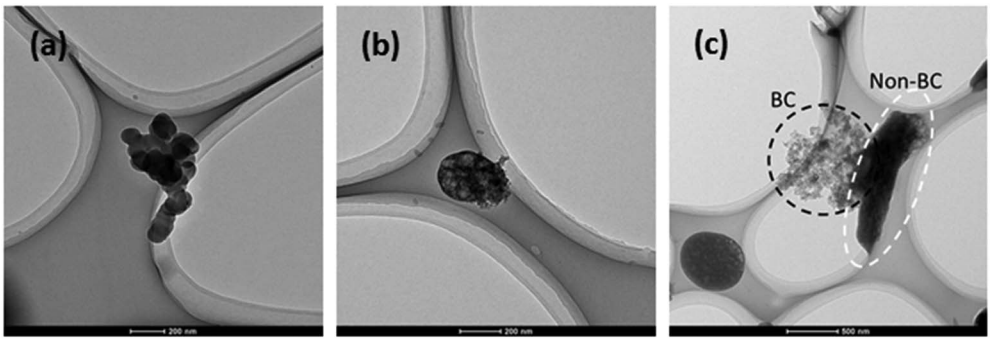

Figure 4. Example TEM images of (a) bare, (b) shell/core, (c) and nonshell/noncore of black carbon (BC) that were collected at a stationary point over the Arctic Ocean on 16 September 2014. The black and white broken circles in Figure 4c denote BC and non-BC materials, respectively. BC in nonshell/noncore type was distinguished from non-BC compounds based on their morphological properties.

4. Conclusions

In this study, we carried out shipborne measurements of rBC aerosol particles over the Arctic Ocean, Bering Sea, and North Pacific Ocean using a SP2 instrument from 31 August 2014 to 9 October 2014. The average rBC concentration in the high-latitude region of $> 70°$N was 1.0 ± 1.2 ng/m^3; given that the transport of aerosols in continental air masses to the Arctic Ocean region was limited during this observation period, this level may have prevailed over the Arctic Ocean. In ambient air over the Arctic Ocean, we also found that a notable fraction (~20%) of the rBC particles had noncore/nonshell structures, as indicated by the lag time analysis that was conducted using SP2. Based on the TEM-EDX analysis, these were likely generated by coagulation with sea-salt particles. Clearly, long-term observations covering all seasons would be required to understand the BC properties over the Arctic Ocean.

Acknowledgments

We thank the crew of the R/V *Mirai*, staff of Global Ocean Development, Inc., and Marine Works Japan, Ltd. for their support with observations throughout the cruise. We also acknowledge K. Uematsu at Marine Works Japan Ltd. for his technical assistance with the individual particle analysis carried out using the TEM. This study was supported by a Grant-in-Aid for Scientific Research Young Scientists (B) 25740013 and partially carried out in the Arctic Challenge for Sustainability (ArCS) Project. The data for this paper are available upon request to the corresponding author.

References

Adachi, K., S. H. Chung, and P. R. Buseck (2010), Shapes of soot aerosol particles and implications for their effects on climate, *J. Geophys. Res.*, *115*, D15206, doi:10.1029/2009JD012868.

Bond, T. C., et al. (2013), Bounding the role of black carbon in the climate system: A scientific assessment, *J. Geophys. Res. Atmos.*, *118*, 5380–5552, doi:10.1002/jgrd.50171.

Chi, J. W., et al. (2015), Sea salt aerosols as a reactive surface for inorganic and organic acidic gases in the arctic troposphere, *Atmos. Chem. Phys. Discuss.*, *15*, 16,715–16,745, doi:10.5194/acpd-15-16715-2015.

Dahlkötter, F., M. Gysel, D. Sauer, A. Minikin, R. Baumann, P. Seifert, A. Ansmann, M. Fromm, C. Voigt, and B. Weinzierl (2014), The Pagami Creek smoke plume after long-range transport to the upper troposphere over Europe—Aerosol properties and black carbon mixing state, *Atmos. Chem. Phys.*, *14*, 6111–6137, doi:10.5194/acp-14-6111-2014.

Dee, D. P., et al. (2011), The ERA-Interim reanalysis: Configuration and performance of the data assimilation system, *Q. J. R. Meteorol. Soc.*, *137*, 553–597, doi:10.1002/qj.828.

Ehara, K., C. Hagwood, and K. J. Coakley (1996), Novel method to classify aerosol particles according to their mass-to-charge ratio: Aerosol particle mass analyzer, *J. Aerosol Sci.*, *27*(2), 217–234.

Eleftheriadis, K., S. Vratolis, and S. Nyeki (2009), Aerosol black carbon in the European Arctic: Measurements at Zeppelin station, Ny-Ålesund, Svalbard from 1998–2007, *Geophys. Res. Lett.*, *36*, L02809, doi:10.1029/2008GL035741.

Flanner, M. G. (2013), Arctic climate sensitivity to local black carbon, *J. Geophys. Res. Atmos.*, *118*, 1840–1851, doi:10.1002/jgrd.50176.

Flanner, M. G., C. S. Zender, P. G. Hess, N. M. Mahowald, T. H. Painter, V. Ramanathan, and P. J. Rasch (2009), Springtime warming and reduced snow cover from carbonaceous particles, *Atmos. Chem. Phys.*, *9*, 2481–2497, doi:10.5194/acp-9-2481-2009.

Gao, R., et al. (2007), A novel method for estimating light-scattering properties of soot aerosols using a modified single-particle soot photometer, *Aerosol Sci. Technol.*, *41*(2), 125–135.

Jacobson, M. Z. (2001), Strong radiative heating due to the mixing state of black carbon in atmospheric aerosols, *Nature*, *409*, 695–697, doi:10.1038/35055518.

Keegan, K. M., M. R. Alberta, J. R. McConnell, and I. Bakera (2014), Climate change and forest fires synergistically drive widespread melt events of the Greenland Ice Sheet, *Proc. Natl. Acad. Sci. U.S.A.*, *111*(22), 7964–7967, doi:10.1073/pnas.1405397111.

Kondo, Y., et al. (2011), Emissions of black carbon, organic, and inorganic aerosols from biomass burning in North America and Asia in 2008, *J. Geophys. Res.*, *116*, D08204, doi:10.1029/2010JD015152.

Liu, J., S. Fan, L. W. Horowitz, and H. Levy II (2011), Evaluation of factors controlling long-range transport of black carbon to the Arctic, *J. Geophys. Res.*, *116*, D04307, doi:10.1029/2010JD015145.

Matsui, H., et al. (2011), Seasonal variation of the transport of black carbon aerosol from the Asian continent to the Arctic during the ARCTAS aircraft campaign, *J. Geophys. Res.*, *116*, D05202, doi:10.1029/2010JD015067.

McConnell, J. R., R. Edwards, G. L. Kok, M. G. Flanner, C. S. Zender, E. S. Saltzman, J. R. Banta, D. R. Pasteris, M. M. Carter, and J. D. W. Kahl (2007), 20th century industrial black carbon emissions altered Arctic climate forcing, *Science*, *317*, 1381–1384.

Miyakawa, T., Y. Kanaya, Y. Komazaki, F. Taketani, X. Pan, M. Irwin, and J. Symonds (2016), Intercomparison between a single particle soot photometer and evolved gas analysis in an industrial area in Japan Implications for the consistency of soot aerosol mass concentration measurements, *Atmos. Environ.*, *127*, 14–21.

Moteki, N., and Y. Kondo (2007), Effects of mixing state on black carbon measurements by laser-induced incandescence, *Aerosol Sci. Technol.*, *41*, 398–417.

Moteki, N., and Y. Kondo (2010), Dependence of laser-induced incandescence on physical properties of black carbon aerosols: Measurements and theoretical interpretation, *Aerosol Sci. Technol.*, *44*, 663–675.

Moteki, N., Y. Kondo, and K. Adachi (2014), Identification by single-particle soot photometer of black carbon particles attached to other particles: Laboratory experiments and ground observations in Tokyo, *J. Geophys. Res. Atmos.*, *119*, 1031–1043, doi:10.1002/2013JD020655.

Myhre, G., et al. (2013), Radiative forcing of the direct aerosol effect from AeroCom Phase II simulations, *Atmos. Chem. Phys.*, *13*, 1853–1877, doi:10.5194/acp-13-1853-2013.

Petzold, A., et al. (2013), Recommendations for reporting "black carbon" measurements, *Atmos. Chem. Phys.*, *13*, 8365–8379, doi:10.5194/acp-13-8365-2013.

Quinn, P. K., et al. (2008), Short-lived pollutants in the Arctic: Their climate impact and possible mitigation strategies, *Atmos. Chem. Phys.*, *8*, 1723–1735, doi:10.5194/acp-8-1723-2008.

Quinn, P. K., et al. (2011), *The Impact of Black Carbon on Arctic Climate*, *AMAP Tech. Rep. 4*, 72 pp., Arctic Monitoring and Assessment Programme (AMAP), Oslo.

Raatikainen, T., D. Brus, A.-P. Hyvärinen, J. Svensson, E. Asmi, and H. Lihavainen (2015), Black carbon concentrations and mixing state in the Finnish Arctic, *Atmos. Chem. Phys. Discuss.*, *15*, 15,621–15,654, doi:10.5194/acpd-15-15621-2015.

Schwarz, J. P., et al. (2006), Single-particle measurements of midlatitude black carbon and light-scattering aerosols from the boundary layer to the lower stratosphere, *J. Geophys. Res.*, *111*, D16207, doi:10.1029/2006JD007076.

Schwarz, J. P., J. R. Spackman, R. S. Gao, L. A. Watts, P. Stier, M. Schulz, S. M. Davis, S. C. Wofsy, and D. W. Fahey (2010), Global-scale black carbon profiles observed in the remote atmosphere and compared to models, *Geophys. Res. Lett.*, *37*, L18812, doi:10.1029/2010GL044372.

Schwarz, J. P., B. H. Samset, A. E. Perring, J. R. Spackman, R. S. Gao, P. Stier, M. Schulz, F. L. Moore, E. A. Ray, and D. W. Fahey (2013), Global-scale seasonally resolved black carbon vertical profiles over the Pacific, *Geophys. Res. Lett.*, *40*, 5542–5547, doi:10.1002/2013GL057775.

Sedlacek, A. J., III, E. R. Lewis, L. Kleinman, J. Xu, and Q. Zhang (2012), Determination of and evidence for non-core-shell structure of particles containing black carbon using the Single-Particle Soot Photometer (SP2), *Geophys. Res. Lett.*, *39*, L06802, doi:10.1029/2012GL050905.

Sharma, S., E. Andrews, L. A. Barrie, J. A. Ogren, and D. Lavoué (2006), Variations and sources of the equivalent black carbon in the high Arctic revealed by long-term observations at Alert and Barrow: 1989–2003, *J. Geophys. Res.*, *111*, D14208, doi:10.1029/2005JD006581.

Sharma, S., M. Ishizawa, D. Chan, D. Lavoué, E. Andrews, K. Eleftheriadis, and S. Maksyutov (2013), 16-year simulation of Arctic black carbon: Transport, source contribution, and sensitivity analysis on deposition, *J. Geophys. Res. Atmos.*, *118*, 943–964, doi:10.1029/2012JD017774.

Shiraiwa, M., Y. Kondo, T. Iwamoto, and K. Kita (2010), Amplification of light absorption of black carbon by organic coating, *Aerosol Sci. Technol.*, *44*(1), 46–54, doi:10.1080/02786820903357686.

Sierau, B., R. Y. -W. Chang, C. Leck, J. Paatero, and U. Lohmann (2014), Single-particle characterization of the high-Arctic summertime aerosol, *Atmos. Chem. Phys.*, *14*, 7409–7430, doi:10.5194/acp-14-7409-2014.

Spackman, J. R., R. S. Gao, W. D. Neff, J. P. Schwarz, L. A. Watts, D. W. Fahey, J. S. Holloway, T. B. Ryerson, J. Peischl, and C. A. Brock (2010), Aircraft observations of enhancement and depletion of black carbon mass in the springtime Arctic, *Atmos. Chem. Phys.*, *10*, 9667–9680, doi:10.5194/acp-10-9667-2010.

Stone, R. S., A. Sharma, A. Herber, K. Eleftheriadis, and D. W. Nelson (2014), A characterization of Arctic aerosols on the basis of aerosol optical depth and black carbon measurements, *Elem. Sci. Anthropocene*, doi:10.12952/journal.elementa.000027.

Takashima, H., M. Shiotani, M. Fujiwara, N. Nishi, and F. Hasebe (2008), Ozonesonde observations at Christmas Island (2°N, 157°W) in the equatorial central Pacific, *J. Geophys. Res.*, *113*, D10112, doi:10.1029/2007JD009374.

Wang, Q., J. P. Schwarz, J. Cao, G. Rushan, D. W. Fahey, H. Tafeng, R.-J. Huang, H. Yongming, and Z. Shen (2014), Black carbon aerosol characterization in a remote area of Qinghai–Tibetan Plateau, western China, *Sci. Total Environ.*, *489–490*, 151–158.

Wofsy, S. C., et al. (2012), HIPPO merged 10-second meteorology, atmospheric chemistry, aerosol data (R_20121129), Carbon Dioxide Inf. Anal. Cent., Oak Ridge Natl. Lab., Oak Ridge, Tenn., doi:10.3334/CDIAC/hippo_010 (Release 20121129).